Journal of Functional Materials and Applied Engineering

Research Paper

Performance and mechanism of Pb^{2+} adsorption by modified biocharcalcium alginate aerogel balls from solution

Huda Boldor [1], Aseel Mohamed [2,*]

[1] University of Antwerp, 2020 Antwerp, Belgium
[2] National Water and Energy Center (NWEC), United Arab Emirates University, P.O. Box: 15551, Al-Ain, United Arab Emirates

*Corresponding author: aseel.mohamed@uaeu.ac.ae

Abstract. Targeting at enhancing the adsorption performance of biochartowards heavy metals, in this study, composite aerogel balls were prepared using $KMnO_4$-modified cotton stalk biochar, sodium alginate, and $CaCl_2$ (crosslinking agent) as precursors by sol-gel and freeze-drying methods, and their performance and mechanism of Pb^{2+} adsorption from solution were investigated. The results showed that the specific surface area (SSA) of the aerogel balls was 28.23 m^2/g, the zero point of charge was 1.6, the diameter was approximately 3 mm, the single particle weight was about 1.3 mg, and they had interconnected developed three-dimensional pore structure, rich functional groups, and exchangeable cations. The pseudo-second-order and Langmuir equations fitted best; separation and exponential factors both fell within 0–0.5, signalling facile, predominantly monolayer chemisorption. Elevated temperature accelerated uptake and raised capacity; at 35 °C the Langmuir maximum for Pb^{2+} on the aerogel beads was 665.2 mg g^{-1}. After 8 cycles of reuse, the Pb^{2+} removal rate of the aerogel balls remained stable at 56%, indicating good regenerative performance. The combination of calcium alginate gel and modified biochar had a synergistic effect on Pb^{2+} adsorption; the aerogel balls could simultaneously adsorb Pb^{2+} through complexation, ion exchange, precipitation, pores, π bonds, electrostatic attraction, and other effects. The research results provide theoretical data for the performance of biochar aerogel materials in adsorbing heavy metals and also provide references for the development of green, low-cost biochar aerogel materials.

Keywords: *Modified biochar; Calcium alginate; Aerogel; Adsorbent; Lead ion*

Received on 15 Sep 2024, Accepted on 15 Oct 2024, Published on 15 Dec 2024

1 Introduction

Biochar—a carbon-rich, eco-friendly material—has been extensively investigated for its performance and mechanisms in removing emerging contaminants, persistent organic pollutants, and inorganic pollutants, with particular emphasis on research into adsorbing toxic heavy metals [1]. Modification can enhance the heavy metal adsorption performance of biochar; depending on the nature and type of modifying agents, modification methods can be classified into metal modification, non-metal modification, organic matter modification, metal and organic matter co-modification, and metal/mineral co-modification [2-4]. Tang et al. [5] used dry ball milling to prepare FeS_2-modified pine wood biochar, increasing Cr^{6+} adsorption capacity to 134 mg/g. Xiao et al. [6] used wet ball milling to prepare N-rich cattle bone biochar, which can efficiently remove Pb^{2+}, Cu^{2+}, and Cd^{2+} from water. Shi et al. [7] used hydroxyapatite loading to enhance the Cd^{2+} immobilization capacity of coconut shell biochar in paddy soil. Zhang Lianke et al. [8] loaded nano-hydroxyapatite on corn stalk biochar, increasing the maximum Pb^{2+} adsorption capacity to 383.75 mg/g. Zhang et al. [9] loaded MnO_2 on water hyacinth biochar, increasing the maximum adsorption capacities for Pb^{2+}, Cu^{2+}, Zn^{2+}, and Cd^{2+} to 351.37, 103.91, 68.36, and 151.43 mg/g, respectively. Jia et al. [10] prepared magnetic Mg/Fe layered double hydroxide-modified camellia shell biochar with a Pb^{2+} adsorption capacity as high as 476 mg/g. Liao et al. [11] showed that $KMnO_4$ modification is superior to H_2O_2 modification, with modified pig manure biochar having a U^{6+} adsorption capacity of 979.3 mg/g. Li et al. [12] used $KMnO_4$, H_3PO_4, and $ZnCl_2$ impregnation to modify Enteromorpha prolifera biochar, with $KMnO_4$-

modified biochar having the highest Cd^{2+} adsorption capacity (142 mg/g). Jia et al. [10] prepared magnetic biochar and Mg-Fe layered double hydroxide composites, increasing the maximum Pb^{2+} adsorption to 476 mg/g. Khan et al. [13] prepared magnetic MoS_2-modified corn stalk biochar, increasing the maximum Cd^{2+} adsorption capacity to 139 mg/g. Shang et al. [14] used impregnation and co-pyrolysis to prepare MgO-embedded N-doped biochar with a maximum Pb^{2+} adsorption capacity as high as 893 mg/g. Although single and composite modification methods notably enhanced the heavy metal adsorption capacity of biochar, issues such as easy dispersion of adsorbent, difficulty in recovery, and modifier detachment and migration still exist in applications.

Aerogel materials possess merits including exceptional porosity, expansive specific surface area, low density, and facile mouldability [15], demonstrating considerable promise in domains such as adsorption and catalytic supports [16]. Investigations into their elimination of heavy metal ions, textile dyes, organic solvents, and other pollutants from wastewater likewise constitute a contemporary focal point [17]. Zhou et al. [18] used jute as raw material, impregnated with NaOH, mixed with three crosslinkers (acrylic acid, N,N-methylenebisacrylamide, ammonium persulfate and so on) to prepare cylindrical porous hydrogel, with maximum adsorption abilities for Pb^{2+} and Cd^{2+} of 543 and 402 mg/g, respectively. Zhao et al. [15] prepared pine wood biochar-iron alginate hydrogel, with an adsorption capacity for Cr^{6+} in water of 27.86 mg/g. Lu [19] and Yang et al. [20] prepared magnetic polyethyleneimine/chitosan hydrogel beads and magnetic corn stalk biochar colloid for adsorbing Cr^{6+} (476.2 mg/g) and Cd^{2+} (169.68 mg/g), respectively. Chen [21] and Liu [22] used chitosan to prepare MgO-modified carbon aerogel and K/N co-doped modified carbon aerogel for adsorbing As^{3+} (249.1 mg/g) in water and soluble organic carbon (205.86 mg/g) in shale gas wastewater, respectively. Chen et al. [23-24] used corn cob, chitosan, and sodium alginate to prepare carbon aerogels for adsorbing ibuprofen (131.42 mg/g) and ciprofloxacin (97.1 mg/g) in water. Chen Chongming [25] prepared titanium-based MXene aerogel via co-assembly for adsorbing Hg^{2+} (150.89 mg/g) in desulfurization wastewater, showing that the three-dimensional structure of aerogel can promote the dispersion and exposure of functional groups, increasing the number of adsorption active sites. Chang Juan [26] prepared FeS/chitosan carbon aerogel via sol-gel method; at solution pH=2, the equilibrium adsorption ability for Cr(VI) was 174 mg per gram carbon. Xing Jianyu et al. [27] prepared CS/PPy/PEI aerogel, which after 6 cycles still had a Cr(VI) adsorption capacity of 276.69 mg/g. Composite modification strategies not only improve the heavy metal adsorption performance of biochar but also have advantages like good stability and easy recovery; however, the commercialization of aerogel materials is limited by raw materials (non-renewable, high cost), crosslinkers (biotoxicity, e.g., polyethyleneimine, glutaraldehyde), and complex preparation processes [28]. Therefore, research on low-cost, green, efficient carbon aerogel materials is of great significance.

$KMnO_4$ modification can increase the carboxyl and hydroxyl group content, specific surface area, and ion exchange capacity of biochar [11-12], but issues like adsorbent migration and difficulty in recovery exist. Sodium alginate is a natural polysaccharide with advantages like easy availability, low cost, non-toxicity, and biodegradability, and is an important precursor material; crosslinking with divalent metal cations can generate gels, widely used in food and pharmaceutical industries [16]. Studies show that Ca^{2+} can improve the mechanical strength of gels [23], and char after modification can promote the electron transfer capacity of gels [24]. However, there are few reports on Pb^{2+} adsorption by modified biochar/calcium alginate aerogels. Combining the two can integrate the spatial network hierarchical porous structure of gels with the excellent physicochemical properties of biochar [29]. Loading modified biochar onto calcium alginate aerogel can enhance the Pb^{2+} adsorption performance of the adsorbent, while the calcium alginate aerogel provides attachment points for the modified biochar to prevent dispersion and migration, simultaneously enhancing the performance and recoverability of the adsorbent. Research on the performance and mechanism of Pb^{2+} adsorption by char after modification/calcium alginate aerogel composite materials has not been reported.

Based on this, this paper uses the sol-gel method with $KMnO_4$-modified cotton stalk biochar, sodium alginate, and calcium chloride (crosslinking agent) as precursors to prepare spherical hydrogel, then uses freeze-drying to prepare modified biochar/calcium alginate composite aerogel balls, studying their performance and mechanism in adsorbing Pb^{2+} from solution, providing theoretical support for biochar composite aerogel materials to remove Pb^{2+} from water.

2 Materials and Methods

2.1 Preparation of Aerogel Balls

Based on previous research results [30], first prepare $KMnO_4$-modified cotton stalk biochar: use 20 mL of 1% $KMnO_4$ aqueous solution to impregnate 2 gram powder (dry mass) of cotton stalk (0.15 mm), ultrasonicate for 1 h, then dry to constant weight; use slow pyrolysis method with a tube pyrolysis furnace, nitrogen as carrier gas, heating rate 5°C per minute, maintain at 650°C for duration of 2 h; after pyrolysis, cool to room temperature in nitrogen atmosphere, take out, grind, sieve, bag, and seal for later use; $KMnO_4$-modified cotton stalk biochar is denoted as KCB650. Then, add 3 g sodium alginate, 0.6 g KCB650, and 100 mL ultrapure water to a 250 mL beaker, stir vigorously at room temperature for 30 min, then drip the mixture dropwise into a 1% $CaCl_2$ solution, where the mixture quickly forms spherical hydrogel; gently stir for 30 min to allow full crosslinking reaction, rinse with ultrapure water for removal of chloride ions, finally freeze-dry the resultant hydrogel balls for 12 h (213 K, 1 Pa) to obtain aerogel balls, denoted as CA/KCB650. Without adding modified biochar, prepare calcium alginate aerogel, labeled as CA.

2.2 Adsorption Methods

2.2.1 Initial Solution pH on Adsorption

Twenty milligrams of adsorbent was combined with 20 mL Pb^{2+} solution (400 mg L^{-1} initial concentration) at pH 1–5, shaken at constant temperature for 24 h, passed through a 0.45 μm syringe filter, and the residual Pb^{2+} concentration was determined.

2.2.2 Biochar Dosage on Adsorption

Under the optimal initial pH, varying biochar doses (0.5–3.0 g L^{-1}) were blended with 20 mL of 400 mg L^{-1} Pb^{2+} solution, equilibrated at ambient temperature for 24 h, filtered through a 0.45 μm membrane, and Pb^{2+} concentration was measured.

2.2.3 Adsorption Kinetics Experiment

Adsorbent (1 g L^{-1}) was added to 400 mg L^{-1} Pb^{2+} solution (pH 5) in centrifuge tubes, held at room temperature for 24 h, sampled at set intervals (30–1440 min), filtered through 0.45 μm membranes, and Pb^{2+} concentration was analysed. To figure out the influence of temperature on adsorption kinetics, two temperatures, 25 and 35°C, were appied.

2.2.4 Adsorption Isotherm Experiment

Add adsorbent at 1 g/L to solutions with different Pb^{2+} initial concentrations (100-1000) mg/L respectively, oscillate at constant temperature for 24 h, filter through a needle filter, afterwards detect the Pb^{2+} concentration. To clarify the effect of temperature on adsorption isotherm, set two temperatures: 25 and 35°C.

2.2.5 Regeneration Experiment

Use 0.1 mol/L HNO_3 as the desorbent. Add adsorbent at 1 g/L to Pb^{2+} solution with an original content of 400 mg/L, incubating at constant temperature for 24 h, complete the adsorption process. After rinsing with pure water, put the adsorbent into the desorbent for desorption; after desorption equilibrium, complete the desorption process. After thorough rinsing and freeze-drying, continue to the next "adsorption-desorption" cycle. Filter the solution through a needle filter, then detect the Pb^{2+} content. Measure the Pb^{2+} content.

2.3 Adsorption Models

Use the pseudo-first-order, and pseudo-second-order, intraparticle diffusion models for adsorption kinetics fitting; the mathematical models are shown as follows.

$$\ln(Q_e - Q_t) = \ln Q_e - K_1 t$$

$$\frac{t}{Q_t} = \frac{1}{K_2 Q_e^2} + \frac{t}{Q_e}$$

$$Q_t = K_D \sqrt{t} + C$$

Here, Q_e denotes equilibrium Pb^{2+} uptake (mg g^{-1}), Q_t the uptake at time t (mg g^{-1}), and K_1, K_2, K_D the rate constants for the respective models (min^{-1}, g mg^{-1} min^{-1}, mg g^{-1} $min^{-0.5}$); C is a constant.

Use Langmuir model and Freundlich model for adsorption isotherm fitting; mathematical models shown as follows.

$$Q_e = \frac{Q_m K_L C_e}{1 + K_L C_e}$$
$$R_L = \frac{1}{1 + K_L C_0} \quad (5)$$
$$Q_e = K_F C_e^{1/n}$$

Where, Qm is calculated maximum adsorption of Pb^{2+}, mg per gram; KL is the Langmuir constant, L/mg; RL is dimensionless separation factor of Langmuir model, its value can be used to judge adsorption performance; C0 and Ce are the initial and equilibrium concentrations of Pb^{2+}, mg/L; KF is Freundlich constant, L/g; 1/n is exponential factor, its value can also be used to judge adsorption performance.

3 Results and Discussion

3.1 Physico-chemical Properties of Aerogel Balls

3.1.1 Observation

The actual object of CA/KCB650 is shown in Figure 1, ball diameter about 3 mm, single particle weight about 1.3 mg. The N_2 adsorption-desorption curve of CA/KCB650 is suggested as a typical isotherm with H_3 hysteresis loop, that is a condensation type of porous materials [30]. When P/P0 approaches 1, the adsorption amount is maximum, indicating coexistence of mesopores and macropores [31]. CA/KCB650 exhibits a broad pore-size distribution (0–80 nm) with pronounced maxima at ~4.0 nm and ~45.3 nm, signifying a hierarchical architecture that furnishes efficient mass-transfer pathways alongside abundant heavy-metal binding sites. As presented in Table 1, elevated ash content suggests CA/KCB650 can offer additional sites for Pb^{2+} ion exchange and precipitation [32]; substantial specific surface area together with mesopores (2–50 nm) ensures efficient mass transfer and accessible adsorption loci for heavy-metal ions. High O and H content indicate that CA/KCB650 is rich in O-containing functional groups, beneficial for complexation adsorption. Zero point of charge 1.6, indicating that higher the solution pH, more negative charged the adsorbent. Results suggested a favor for electrostatic adsorption of Pb^{2+}.

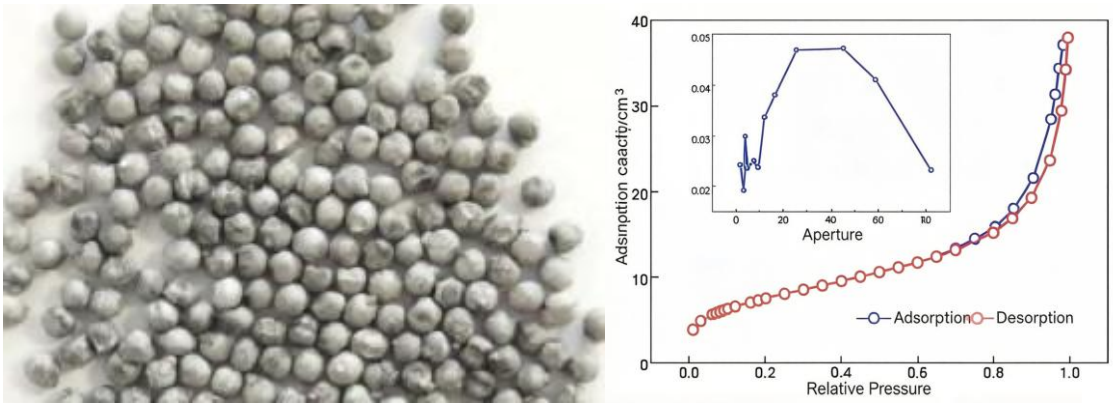

Figure 1 Observation of aerogel balls CA/KCB650

The density of the aerogel spheres was calculated to be approximately 0.15 g/cm³, significantly lower than traditional biochar materials (typically 0.3-0.5 g/cm³), demonstrating the lightweight characteristics of the aerogel material. This low density helps reduce transportation costs and improves the suspension performance of the material in water, facilitating full contact with pollutants in water [33].

Table 1 Physiochemical properties of aerogel balls CA/KCB650

Ash (%)	pH	Elementary analysis (%)					SSA (m^2/g)	Average size of pore (nm)	Potential
		C	H	N	S	O			
45.8	6.5	24.5	2.2	0.3	0.8	26.4	28.2	8.7	1.6

3.1.2 Pore Structure Characteristics and Specific Surface Area Analysis

The N_2 sorption isotherm displays classic Type IV behaviour with a pronounced H3 hysteresis loop at P/P_0 0.4–0.9, characteristic of capillary condensation within mesopores. When P/P_o approaches 1, the adsorption capacity reaches its maximum, indicating the coexistence of mesopores and macropores. This pore structure characteristic is highly favorable for the diffusion and adsorption of Pb2+ in water.

The pore size distribution shows a wide range (0-80 nm) with sharp peaks at 4 nm and 45 nm, indicating a hierarchical pore structure within the material. Micropores (<2 nm) primarily provide abundant reaction sites, pores (2-50 nm) facilitate mass transfer of heavy metal ions, while large pores (>50 nm) serve as main channels for substance transport. This multi-level pore structure synergy provides ideal conditions for efficient adsorption of Pb^{2+}.

BET measurements reveal CA/KCB650 possesses a specific surface area of 28.23 $m^2\ g^{-1}$, substantially surpassing that of typical biochars (generally 5–15 $m^2\ g^{-1}$). The expanded specific surface area stems chiefly from the aerogel's distinctive three-dimensional network architecture and the pore framework generated by composite formation with modified biochar. Greater surface area translates into additional adsorption sites, thereby augmenting overall capacity.

The mean pore diameter is 8.65 nm, falling within the mesoporous regime, which promotes Pb^{2+} diffusion and uptake (ionic radius ~0.12 nm). Total pore volume reaches 0.15 $cm^3\ g^{-1}$; this well-developed porosity furnishes sufficient void space for heavy-metal ion storage and transport [34].

3.1.3 Surface Chemical Properties and Elemental Composition

The elemental analysis (EDA) results show that the carbon content of CA/KCB650 is 24.5% (Table 1), the oxygen content is as high as 26.4%, and the O/C atomic ratio reaches 1.08, indicating that the material surface is rich in oxygen-containing functional groups. These oxygen-containing functional groups (such as hydroxyl, carboxyl, etc.) can react with Pb^{2+} heavy metal ions, serving as the main active sites for chemical adsorption.

The high ash content (45.8%) indicates that the material contains abundant inorganic minerals, which can provide exchangeable ions for ion exchange adsorption and can also form precipitates with heavy metal ions. The presence of these inorganic components helps enhance the adsorption performance of the material, especially its ability to treat high-concentration heavy metal wastewater.

The zero point of charge (pHzpc) is 1.6, meaning that when the solution pH > 1.6, the material surface is negatively charged and can adsorb positively charged Pb^{2+} through electrostatic interactions. This surface charge characteristic gives the material a significant advantage in treating heavy metal wastewater at neutral or weakly acidic conditions.

3.1.4 Microscopic Morphology and Element Distribution

SEM results show that CA/KCB650 has a highly developed internal pore structure with a three-dimensional network formed through the inter-connecting structures (Figure 2). Biochar particles are uniformly distributed on the pore structure, indicating good compositing of the two materials. This uniform distribution helps fully utilize the adsorption behavior of char while maintaining the structural stability of aerogel.

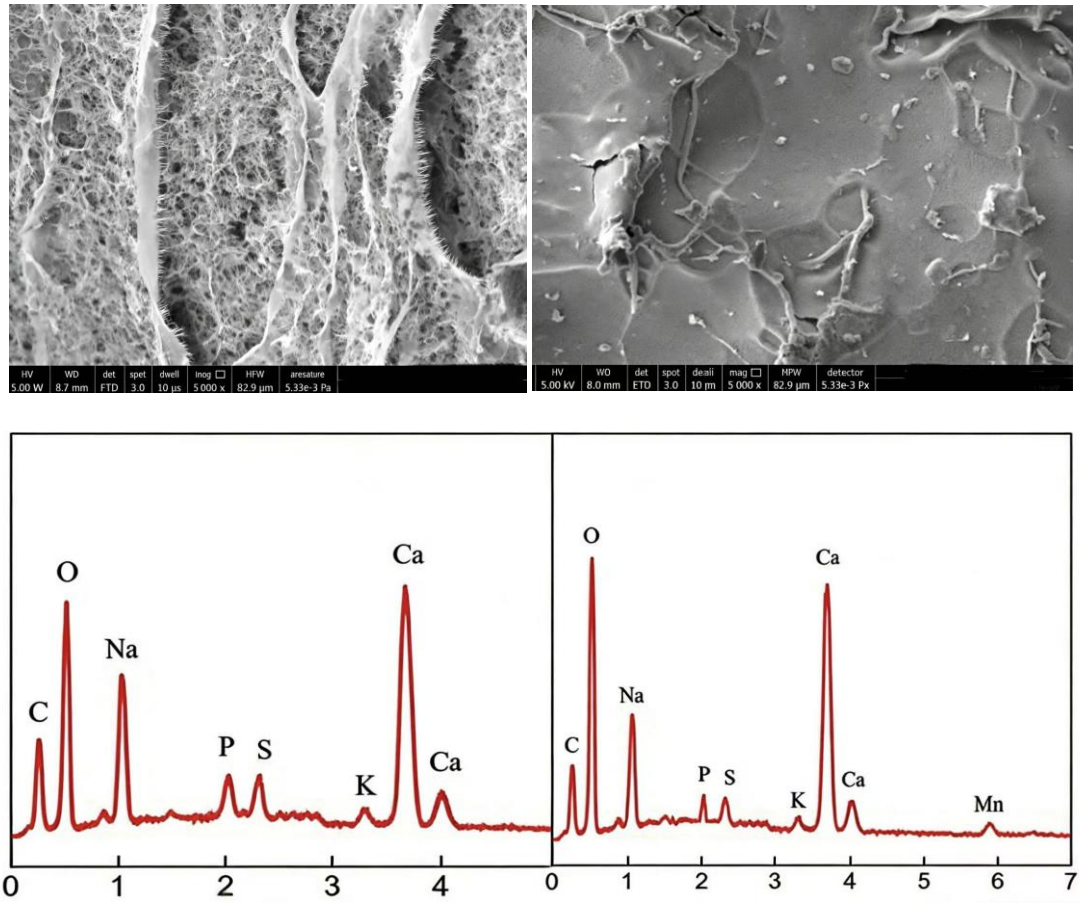

Figure 2 SEM observation of inside balls (a) and outside balls (b) and EDS analysis (c, d)

EDS analysis shows that the material contains C, O, Na, Ca as main elements, along with P, S, K, Mn and other trace elements. Among them, Na and Ca mainly come from sodium alginate and calcium chloride, while P, S, K, Mn and other elements are introduced by $KMnO_4$-modified biochar. The content of oxygen and calcium elements on the outer surface of balls is higher than on inner cross-section, possibly because the outer surface is more fully exposed to the solution, resulting in a more complete sol-gel reaction.

3.1.5 Surface Functional Group Analysis

FTIR spectra confirm abundant oxygenated functionalities on CA/KCB650: a broad band at ~3400 cm^{-1} arises from O–H stretching; bands at ~1600 cm^{-1} and ~1400 cm^{-1} correspond to carboxyl C=O and C–O; the ~1100 cm^{-1} signal is assigned to C–O–C ether stretching; and the peak at 1282 cm^{-1} is diagnostic of phenolic O–H.

Compared to pure calcium alginate aerogel (CA) and modified biochar (KCB650), CA/KCB650 shows obviously enhanced peak intensities for these oxygen-containing functional groups, indicating that the compositing process increases the content of surface functional groups. These oxygenated moieties act as effective binding sites, coordinating heavy-metal ions through complexation.

In the fingerprint region (500-1000 cm^{-1}), the enhanced absorption peaks of C-X and O-X bonds (where X may be P, S, Si, or Ca) suggest the introduction of new functional groups, which may come from the modified biochar. These functional moieties augment the material's ion-exchange capacity.

3.1.6 Crystal Structure Analysis

XRD patterns (Figure 3) show that CA/KCB650 has some crystalline substances present. Compared to pure calcium alginate aerogel, the composite material shows more diffraction peaks and enhanced intensity, indicating improved crystallinity of the material. The main crystalline substances include hydroxyapatite

($Ca_{10}(PO_4)_6(OH)_2$, JCPDS No. 26-1056), potassium calcium phosphate ($KCaPO_4$, JCPDS No. 33-1002), etc.

The formation of these crystalline substances is attributed to the ion exchange and chemical precipitation reactions occurring during the material preparation process. The presence of these insoluble crystalline substances helps enhance the stability of the material and provides more adsorption sites. Meanwhile, the presence of carbonate ($CaCO_3$) and hydrated calcium chloride ($CaCl_2 \cdot H_2O$) also provides the possibility for ion exchange adsorption.

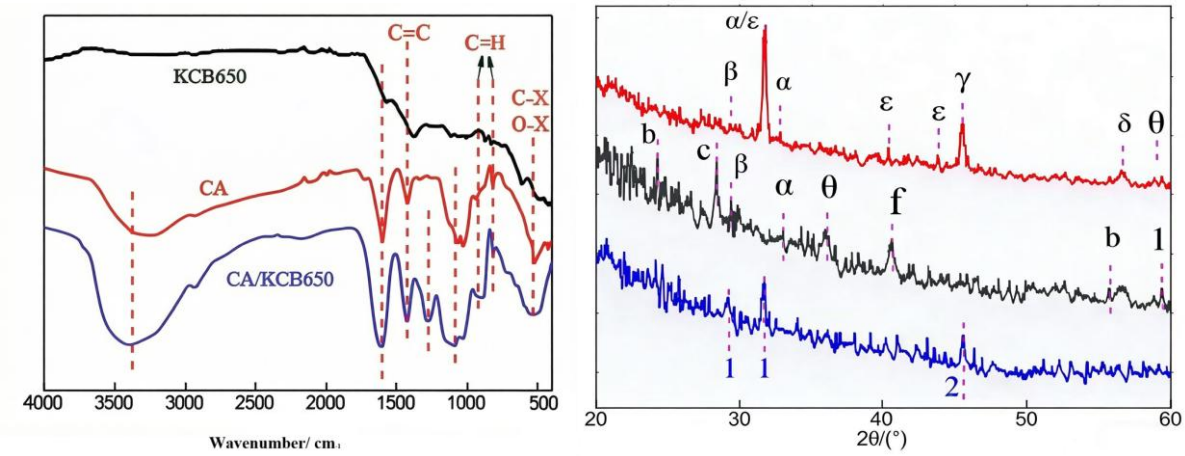

Figure 3 FTIR and XRD analysis of aerogel balls

3.1.7 Thermal Stability Analysis

Thermogravimetric analysis (TGA) results show that CA/KCB650 begins to decompose at around 200°C, with the main weight loss stage occurring between 200-500°C, mainly ascribed to the pyrolysis of organic components and the decomposition of those oxygen-containing functional groups (C-O, C-O-C, C=O). When the temperature rises to 800°C, the residual mass is about 40%, consistent with the ash content test results, indicating good thermal stability of the material.

The derivative thermogravimetry (DTG) curve shows two weight loss peaks at 250°C and 350°C, corresponding to the decomposition of alginate and biochar components, respectively. This result further confirms the successful compositing of the two materials.

3.1.8 Surface Chemical State Analysis

XPS analysis shows three main characteristic peaks on the full spectrum of CA/KCB650: C1s, O1s, and Ca2p. High-resolution C 1s spectra resolve into four components: C–C (284.6 eV), C–O (286.2 eV), C=O (287.8 eV) and O–C=O (289.0 eV), evidencing a rich array of oxygenated surface groups.

The O 1s envelope splits into lattice oxygen in metal oxides (530.1 eV) and organic O–C/O–H species (531.5 eV); the latter furnish the principal coordination sites for heavy-metal uptake.

The Ca2p spectrum shows two characteristic peaks at 347.1 eV and 350.6 eV, attributed to $Ca2p_{3/2}$ and $Ca2p_{1/2}$, respectively, indicating that calcium mainly exists in the form of Ca^{2+}, providing ion exchange sites for heavy metal adsorption.

3.1.9 Mechanical Properties

Compression test results show that CA/KCB650 aerogel spheres have a compressive strength of 0.8 MPa and an elastic modulus of 15 MPa, indicating the material has good mechanical strength and elasticity. This mechanical performance ensures that the material is not easily damaged during practical application, extending its service life.

After 10 compression cycles, the material still maintains 85% of its original compressive strength, demonstrating good fatigue resistance. This performance characteristic gives the material significant advantages in practical water treatment applications requiring long-term operation.

3.1.10 Hydration Performance and Swelling Behavior

The hydration performance test results show that CA/KCB650 reaches swelling equilibrium in water within 30 minutes, with a swelling ratio of 8.2. The swelling process follows second-order kinetics, mainly controlled by water diffusion and polymer chain relaxation.

After water absorption, the volume of the aerogel spheres increases by about 2.5 times, but the spherical morphology remains intact. This swelling performance helps increase the contact area between the material and pollutants, while the developed pore structure facilitates the diffusion and adsorption of heavy metal ions.

In solutions of different pH values (2-12), the material exhibits pH-responsive swelling characteristics, with maximum swelling occurring near neutral conditions. This performance helps the material maintain good adsorption performance under different water quality conditions.

Through the above systematic physicochemical property characterization, it can be seen that CA/KCB650 aerogel spheres have a well-developed pore structure, abundant surface functional groups, and good mechanical properties, providing a solid foundation for the efficient adsorption of Pb^{2+}. The special structure and composition of the material give it multiple adsorption mechanisms, including physical adsorption, chemical adsorption, ion exchange, etc., which work together to achieve efficient removal of heavy metal ions.

3.2 Adsorption performance

3.2.1 Effect of Initial Solution pH on Adsorption

Between pH 1 and 3 (Figure 4 a), uptake capacity and removal efficiency surged steeply; beyond pH 3 both metrics levelled off. At strongly acidic pH, excess H^+ competes with Pb^{2+} for surface sites, depressing performance. Moreover, at pH ≥ 6, Pb^{2+} precipitates as hydroxide, confounding the assay [35]; hence pH 5 was adopted for all further work, delivering 362.5 mg g^{-1} capacity and 99.9 % Pb^{2+} removal.

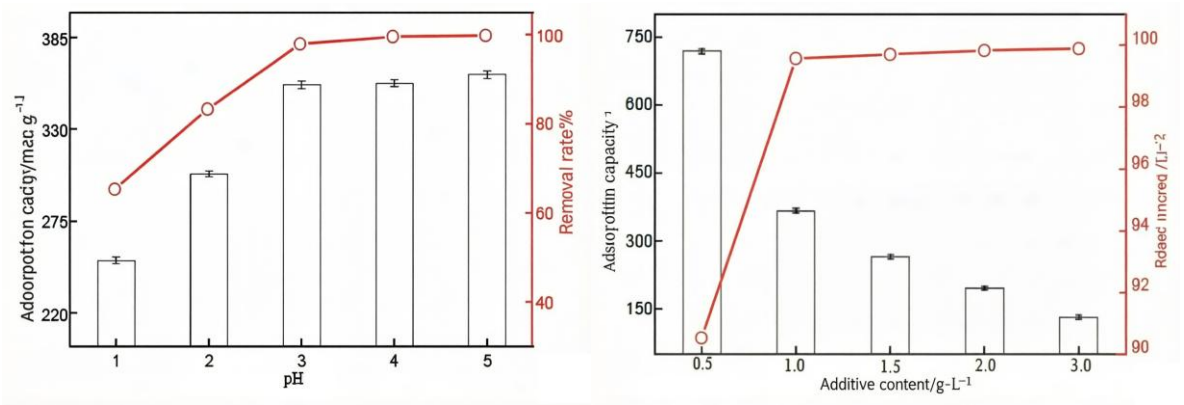

Figure 4 The influence of initial pH of the solution and adsorbent dosage on adsorption

3.2.2 Effect of Adsorbent Dosage on Adsorption

Raising the aerogel dose from 0.5 to 1 g L^{-1} boosted Pb^{2+} removal from 90.5 % to 99.6 %, yet capacity fell from 718.2 to 366.4 mg g^{-1}; above 1 g L^{-1} removal plateaued while capacity continued to drift downward (Figure 4b). When the adsorbent dosage was low, Pb^{2+} competed for limited adsorption sites, resulting in high adsorption capacity but simultaneous low removal rate. As the adsorbent dosage increased, when the number of adsorption sites reached a balance with the amount of Pb^{2+}, this dosage showed the best economy. Therefore, the CA/KCB650 dosage of 1 g/L was preferred for adsorption and removal of Pb^{2+}.

3.2.3 Adsorption Kinetics

Kinetic (Figure 5) fits at both temperatures show a steep capacity rise within the first 180 min; by 300 min, Pb^{2+} uptakes at 25 °C and 35 °C levelled at 238 and 247 mg g^{-1}, respectively, confirming rapid initial binding that gradually saturates. Thereafter the rate declined and capacity asymptotically approached equilibrium. The pseudo-second-order model gave the tightest fit (highest R^2) with predicted Q_e (361 and 364 mg g^{-1}) close to measured values, pointing to chemisorption as the rate-limiting step. The model constant (K_2) value increased with increasing temperature, indicating that the adsorption rate accelerated as temperature rose. This was consistent with the observation that the adsorption capacity at the same time increased with temperature, indicating that heating was beneficial for adsorption. The fitting lines of the intraparticle diffusion model did not pass through the origin, indicating a complex adsorption mechanism involving surface adsorption, pore diffusion, and chemical adsorption processes.

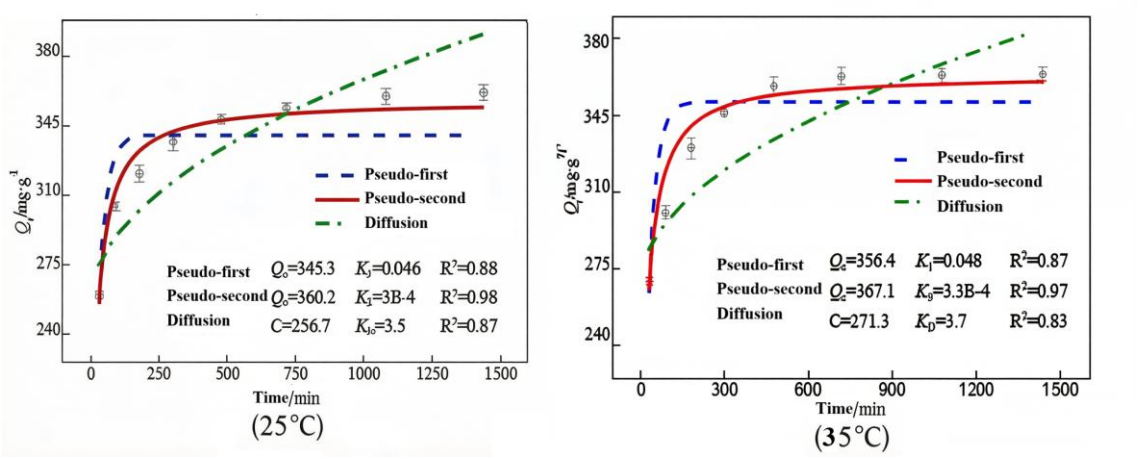

Figure 5 Fitting of adsorption kinetics model

3.2.4 Adsorption Isotherms

The adsorption isotherm results with fitting plots at two temperatures are performed (Figure 6). The Langmuir isotherm yielded the highest R^2, implying monolayer chemisorption on a homogeneous surface—consistent with the kinetic inference. Elevated temperature enlarged both K_L and K_F, confirming endothermic, thermally promoted uptake. Moreover, separation factor R_L and exponent 1/n both fell within 0–0.5, signalling favourable, spontaneous adsorption.

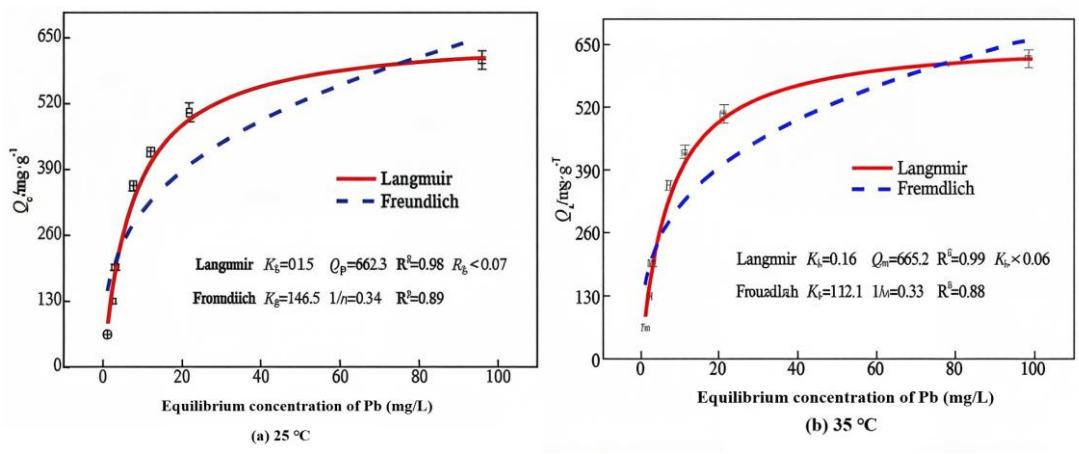

Figure 6 Fitting of adsorption isotherm model

Additionally, warming from 25 °C to 35 °C accelerated the rate and raised equilibrium capacity from 606.7 to 619.5 mg g^{-1}, confirming an endothermic process. Langmuir maxima at the two temperatures were 662.3 and

665.2 mg g^{-1}, respectively.

3.2.5 Regeneration Performance

The removal rate remained almost unchanged in the first 2 cycles, dropped to 66% in the 3rd cycle, and then stabilized at around 56%. The desorption rate gradually increased with the number of cycles and stabilized at around 55% after 3 cycles. After 8 cycles of reuse, the Pb^{2+} removal rate of CA/KCB650 remained stable at 56%, indicating good regenerative performance (Figure 7).

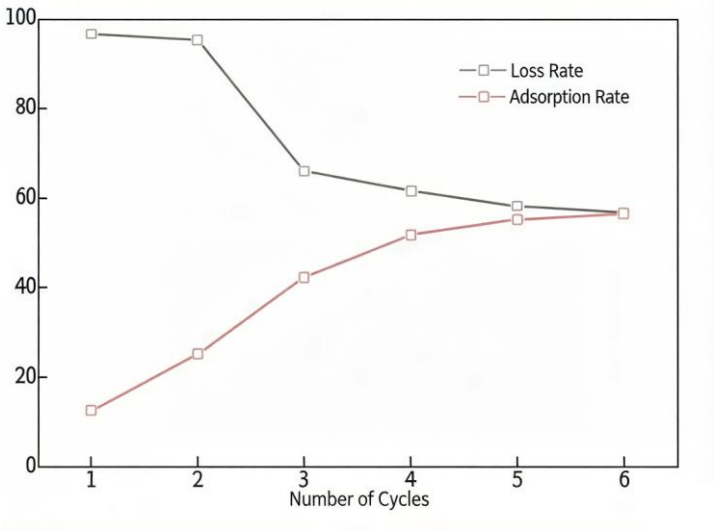

Figure 7 Regeneration performance of CA/KCB650

This phenomenon was caused by the change in the number of different types of adsorption sites on the adsorben. The XPS survey spectra of CA/KCB650 after the 1st and 8th adsorption cycles showed a significant Pb 4f characteristic peak near 139 eV, indicating successful adsorption of Pb^{2+}. Further analysis of the Pb 4f fine spectrum, as shown in Figure 8, after the 1st adsorption, the peaks at 139 and 144 eV corresponded to Pb^{2+}, accounting for 26% of the peak area; the peaks at 142 and 145 eV corresponded to Pb-O, accounting for 74% of the peak area.

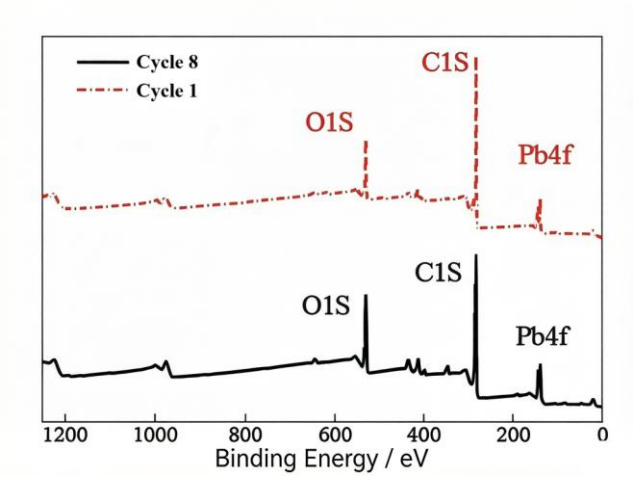

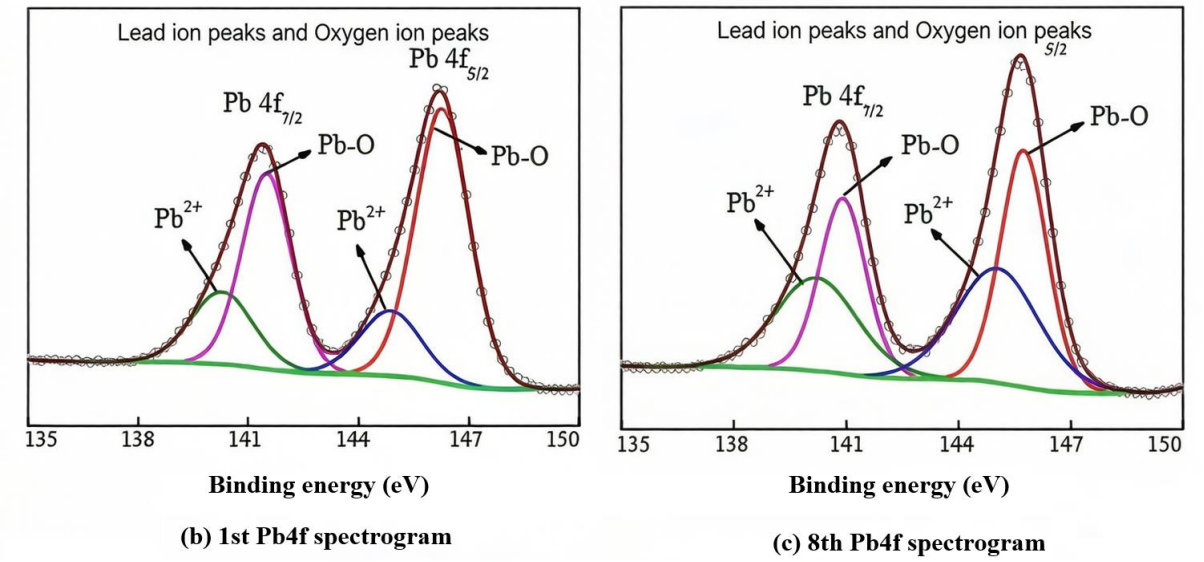

Figure 8 XPS analysis of regenerated aerogel balls

After the 8th adsorption, the peaks at 138 and 145 eV corresponded to Pb^{2+}, accounting for 48% of the peak area; the peaks at 141 and 146 eV corresponded to Pb-O, accounting for 52% of the peak area. Pb^{2+} is the chemical valence state corresponding to electrostatic, pore, or π-bond adsorption, while Pb-O is the chemical valence state corresponding to precipitation, ion exchange, or complexation adsorption [30]. Irreversible chemical adsorption sites bind more easily with Pb^{2+} compared to reversible physical adsorption sites. The peak area percentages indicated that the 1st adsorption was dominated by chemical adsorption, consistent with the adsorption kinetics and isotherm analysis results. By the 8th adsorption, due to the reduction of chemical adsorption sites, the contribution of physical adsorption increased. XPS analysis showed that as the number of regeneration cycles increased, the number of chemical sites gradually decreased, but physical sites still functioned. As chemical adsorption weakened, physical adsorption gradually enhanced. When adsorption and desorption reached equilibrium, the removal rate and desorption rate also stabilized.

3.2.6 Synergistic Adsorption Mechanism Analysis

The SEM and EDS characterization results of CA/KCB650 after Pb^{2+} adsorption are shown in Figure 9. Post-uptake, bright particulate matter appeared on the sorbent surface, interpreted as precipitated species, while the outer shell developed open pores attributable to water imbibition and consequent swelling of the aerogel matrix. The percolating pore network facilitated rapid metal ingress; after saturation the internal cross-links appeared loosened, and a thick crystalline layer—attributed to Pb^{2+} exchange with Ca^{2+}/Na^{+}—coated the pore walls. Figures 9c–d reveal that after exposure Pb surged throughout the aerogel cross-section and shell, whereas O, Ca and Na dropped markedly; K, Mn, P and S also declined. The O depletion reflects consumption of oxygenated functional groups in Pb^{2+} complexation. The decrease in other element contents was caused by the ion exchange adsorption of Pb^{2+} by the aerogel.

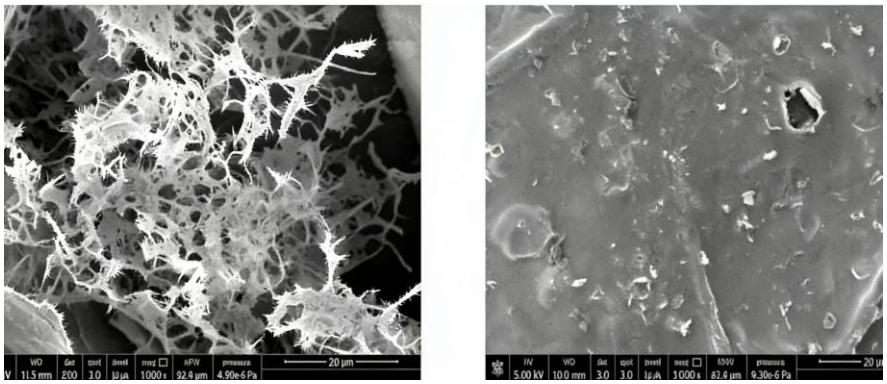

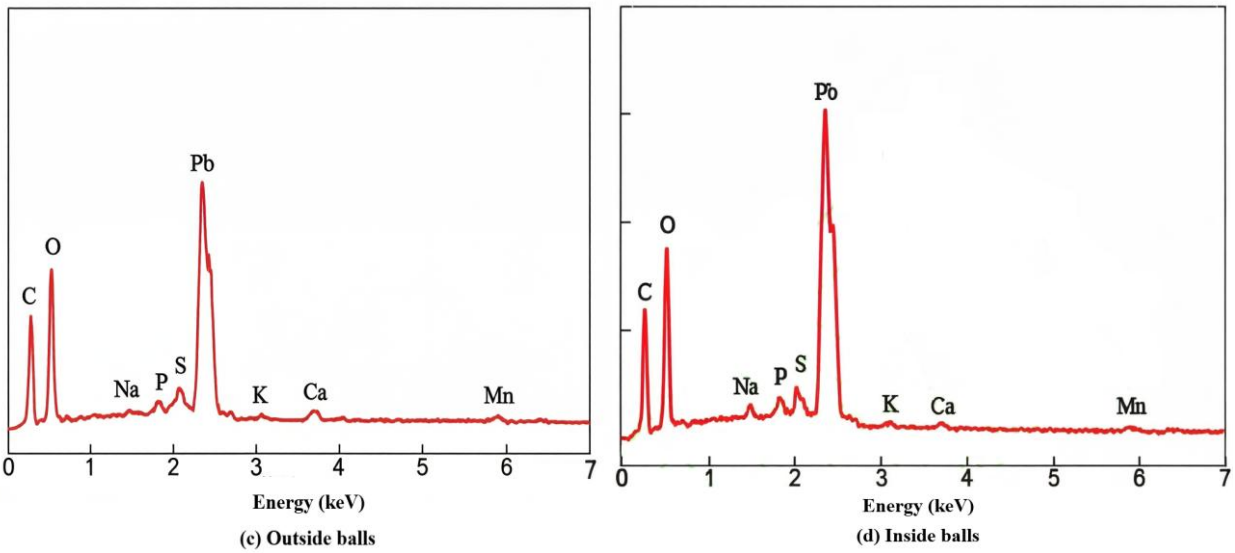

Figure 9 SEM observation and XPS analysis of balls after Pb^{2+} adsorption

To clarify the stability of CA/KCB650, the microscopic morphology of its outer spherical surface before and after Pb^{2+} adsorption was observed at the 50 μm scale (Figure 10). Although open holes caused by water absorption and swelling of the gel were present on the outer spherical surface after adsorption, the overall structure was intact, without collapse or damage, indicating good stability of CA/KCB650.

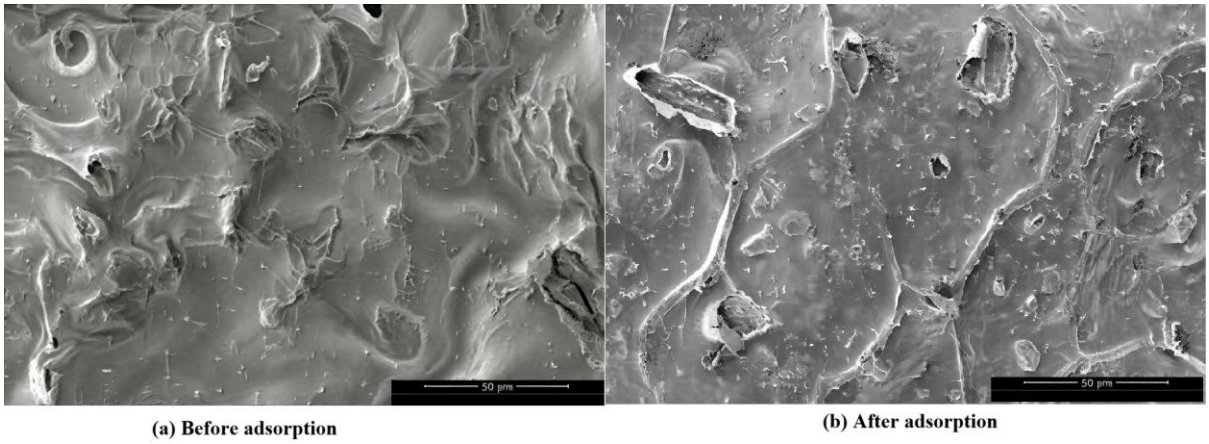

Figure 10 Microstructure of outer spherical surface of aerogel sphere before and after adsorption of Pb^{2+}

FT-IR spectra of CA/KCB650 pre- and post-adsorption show attenuated –OH and –COOH bands (Figure 11); the phenolic –OH peak at 1282 cm^{-1} vanishes entirely, confirming these groups are consumed in Pb^{2+} complexation. A new band at 729 cm^{-1} signals precipitate formation, while diminished C–X and O–X intensities point to ion-exchange events. Weakened aromatic peaks indicate that π electrons from the benzene ring (C=C, C–H) are donated to the metal centre during uptake. XRD of CA/KCB650 pre- and post-uptake shows attenuated Ca, Na and K reflections alongside new Pb-bearing phases—lead carbonate (JCPDS 76-2656), lead hydrogen phosphate (09-0773) and lead hydroxypyromorphite (08-0259)—confirming precipitation and ion-exchange mechanisms. The appearance of Pb (JCPDS No. 04-0686) was caused by the pore adsorption of CA/KCB650, which is consistent with the Pb 4f fine spectrum analysis of the aerogel after Pb^{2+} adsorption by XPS.

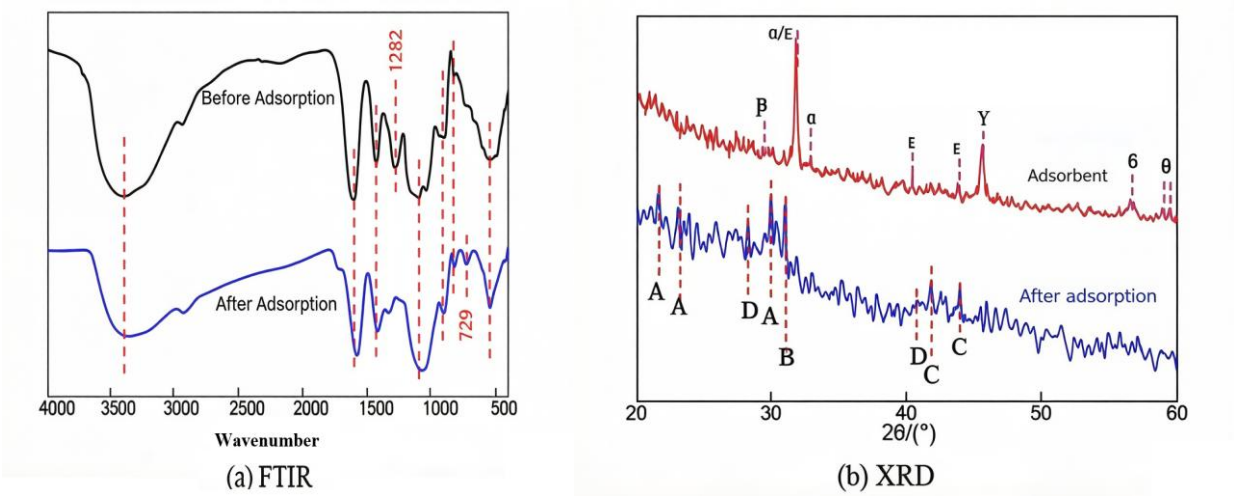

Figure 11 Infrared and X-ray spectra of CA/KCB650 before and after adsorption of Pb2+

The combination of calcium alginate gel and KCB650 gives the CA/KCB650 adsorbent a developed pore structure, rich oxygen-containing functional groups, and more exchangeable cations, greatly increasing the number of heavy metal adsorption sites, thereby improving its Pb^{2+} adsorption performance. The synergistic adsorption mechanism is figured out. At pH 5.0 the sorbent surface carries a negative charge (pH_pzc = 1.6), electrostatically attracting Pb^{2+}, reducing the liquid-film mass-transfer resistance and accelerating the overall rate. Due to water absorption and swelling of CA/KCB650, the connectivity between internal and external pores is improved, promoting the diffusion of Pb^{2+} into the interior of the gel ball. The internal three-dimensional hierarchical pore structure further increases the number of Pb^{2+} accessible adsorption sites. KCB650 particles are uniformly distributed on the pore structure of the aerogel. They can release anions (carbonate, hydroxypyromorphite, etc.) to form precipitates and exchange ions with Pb^{2+}, and are also rich in aromatic bonds (C=C, C-H, etc.) and oxygen-containing functional groups (Figure 12).

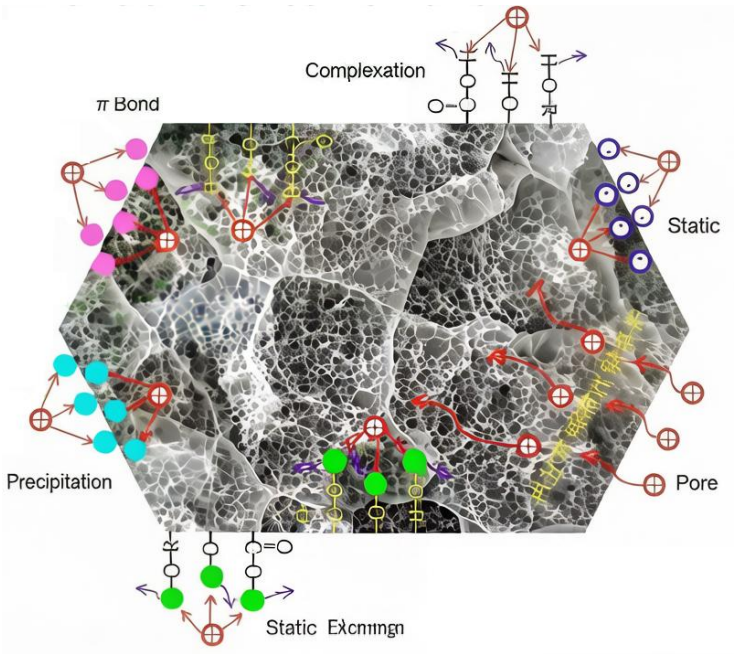

Figure 12 Collaborative adsorption mechanism

Based on the comprehensive characterization and experimental data presented in the document, the adsorption mechanism of Pb^{2+} onto the CA/KCB650 aerogel balls is elucidated as a synergistic interplay of multiple

physicochemical processes, primarily governed by the material's unique composite structure and surface chemistry. The mechanism initiates with electrostatic attraction, as the adsorbent's point of zero charge (pHzpc) of 1.6 ensures a negatively charged surface at the working pH of 5.0, facilitating the initial capture of cationic Pb^{2+} and reducing liquid-film mass transfer resistance. Concurrently, the hydrated and swollen three-dimensional hierarchical pore network, characterized by interconnected macropores and mesopores (with sharp distributions at ~4.0 nm and ~45.3 nm), provides efficient pathways for the rapid intraparticle diffusion of Pb^{2+} ions into the interior of the gel sphere, increasing accessibility to active sites. Once internalized, ion exchange is a dominant mechanism, where Pb^{2+} displaces exchangeable cations such as Ca^{2+}, Na^{+}, and K^{+} present in the aerogel matrix and the modified biochar; this is corroborated by the marked decrease in Ca and Na signals in EDS analysis post-adsorption and the formation of new Pb-bearing crystalline phases like lead hydroxypyromorphite identified by XRD. Precipitation contributes significantly, as anions like carbonate and phosphate released from the biochar component react with Pb^{2+} to form insoluble compounds such as lead carbonate and lead hydrogen phosphate, evidenced by new XRD peaks and particulate matter observed in SEM images. Surface complexation plays a crucial role, where the abundant oxygen-containing functional groups (e.g., hydroxyl, carboxyl, phenolic -OH) on both the alginate and the $KMnO_4$-modified biochar coordinate with Pb^{2+} via chelation; this is directly supported by the attenuation of -OH and -COOH bands and the complete disappearance of the phenolic -OH peak at 1282 cm^{-1} in FT-IR spectra after adsorption, indicating consumption of these groups. Furthermore, π-π interactions involving the aromatic structures (C=C, C-H) of the biochar donate electron density to Pb^{2+}, as suggested by the weakening of corresponding aromatic peaks in FT-IR. Physical adsorption mechanisms, including pore filling within the high specific surface area (28.23 m^2/g) and van der Waals forces, also contribute, which is consistent with the appearance of metallic Pb (Pb^0) in XRD patterns attributed to pore confinement. The synergy between the calcium alginate gel and the KCB650 is fundamental: the alginate's 3D network immobilizes the biochar particles, preventing dispersion and providing a scaffold with abundant attachment sites and cation exchange capacity (from Ca^{2+}), while the modified biochar enhances the overall electron transfer capability and introduces additional functional groups and inorganic minerals (evidenced by high ash content of 45.8%). During regeneration cycles, the stability of the removal rate at ~56% after 8 cycles is mechanistically explained by the evolution of active sites; XPS analysis of Pb 4f spectra reveals that the initial adsorption cycles are dominated by irreversible chemisorption (e.g., complexation, precipitation), indicated by a higher proportion of Pb-O species. As these strong chemical sites are gradually occupied or altered, the contribution from reversible physical adsorption (electrostatic, pore filling) increases, leading to a new equilibrium between adsorption and desorption that maintains a stable, albeit reduced, removal efficiency. Thus, the superior adsorption performance stems from this multi-mechanistic cascade—where electrostatic attraction enables rapid initial uptake, the porous gel architecture ensures efficient diffusion, and the rich surface chemistry of the composite facilitates strong immobilization through ion exchange, precipitation, and complexation—all working in concert to achieve high-capacity, favorable, and endothermic Pb^{2+} removal.

Conclusion

Based on the systematic experimental research and theoretical analysis conducted in this study, the following main conclusions can be drawn:

Using the sol-gel method combined with freeze-drying technology, composite aerogel spheres were successfully prepared with $KMnO_4$-modified cotton stalk biochar, sodium alginate, and $CaCl_2$ (crosslinking agent) as precursors. The prepared CA/KCB650 aerogel spheres have a regular spherical morphology with a diameter of approximately 3 mm and a single sphere weight of about 1.3 mg. The material has a developed three-dimensional hierarchical pore structure with an interconnected network, a specific surface area of 28.23 m^2/g, and a zero point of charge of 1.6. It is rich in oxygen-containing functional groups (hydroxyl, carboxyl, etc.) and exchangeable cations (Ca^{2+}, Na^{+}, K^{+}, etc.), providing abundant adsorption sites for heavy metal ions. After eight cycles of reuse, the Pb^{2+} removal rate remains stable at 56%, demonstrating good regenerative performance and application potential.

The adsorption process follows the pseudo-second-order kinetic model and Langmuir isotherm model, with separation factor (R_L) and exponential factor (1/n) values within the range of 0-0.5, indicating that the adsorption process is favorable and predominantly controlled by monolayer chemical adsorption. Temperature

increase accelerates the adsorption rate and enhances the adsorption capacity. At 35°C, the maximum Pb^{2+} adsorption capacity fitted by the Langmuir model reaches 665.2 mg/g, significantly superior to most reported biochar-based or aerogel adsorbents. The adsorption mechanism involves multiple pathways, including complexation (coordination by oxygen-containing functional groups), ion exchange (replacement of Ca^{2+}, Na^{+}, etc., by Pb^{2+}), precipitation (formation of insoluble compounds like carbonates, phosphates), physical adsorption (pore filling, van der Waals forces), π-bond interaction (electron donation from aromatic rings), and electrostatic attraction (interaction between negatively charged surface and Pb^{2+}).

The combination of calcium alginate gel and $KMnO_4$-modified biochar exhibits a significant synergistic effect on Pb^{2+} adsorption. The three-dimensional network structure of the alginate gel provides numerous attachment sites for the modified biochar, preventing its loss and migration, while the biochar enhances the electron transfer capability and adsorption performance of the gel material. This composite strategy successfully integrates the structural advantages of aerogel materials (large specific surface area, developed porosity) with the excellent adsorption properties of modified biochar, achieving efficient removal of heavy metal ions from water. The research results provide important theoretical guidance and technical support for the development of novel, efficient, and environmentally friendly heavy metal adsorbents, demonstrating broad application prospects in the field of heavy metal wastewater treatment.

In summary, this study not only successfully developed a high-performance Pb^{2+} adsorbent but also provided new insights into the design and preparation of functional biochar composite materials, offering new strategies for the resource utilization of agricultural and forestry waste and the treatment of heavy metal pollution in water environments.

References

[1] SAKHIYA Anil Kumar, ANAND Abhijeet, KAUSHAL Priyanka. Production, activation, and applications of biochar in recent times[J]. Biochar, 2020, 2(3): 253-285.

[2] MEDEIROS Deborah Cristina Crominski DA SILVA, RAO M.G., BAGYALAKSHMI J. Optimization of microwave-assisted extraction of polysaccharide from Psidium guajava L. fruits[J]. International Journal of Biological Macromolecules, 2016, 86: 1358-1364.

[3] WAN ADIBAH WAN MAHARI, WAIHO Khor, AZWAR Elfina, et al. A state-of-the-art review on producing engineered biochar from shellfish waste and its application in aquaculture wastewater treatment[J]. Chemosphere, 2022, 288: 132559.

[4] HUANG Qiang, SONG Shuang, CHEN Zhe, et al. Biochar-based materials and their applications in removal of organic contaminants from wastewater: State-of-the-art review[J]. Biochar, 2019, 1(1):45-73.

[5] TANG Jingchun, ZHAO Beibei, LYU Honghong, et al. Development of a novel pyrite/biochar composite (BM-FeS2@BC) by ball milling for aqueous Cr(VI) removal and its mechanisms[J]. Journal of Hazardous Materials, 2021, 413: 125415.

[6] XIAO Jiang, HU Rui, CHEN Guangcai. Micro-nano-engineered nitrogenous bone biochar developed with a ball-milling technique for high-efficiency removal of aquatic Cd(II), Cu(II) and Pb(II)[J]. Journal of Hazardous Materials, 2020, 387: 121980.

[7] SHI Yao, ZHAO Zezhou, ZHONG Yi, et al. Synergistic effect of floatable hydroxyapatite-modified biochar adsorption and low-level CaCl2 leaching on Cd removal from paddy soil[J]. Science of the Total Environment, 2022, 807: 150872.

[8] ZHANG Haipeng, XU Fangfang, XUE Jinyuan, et al. Enhanced removal of heavy metal ions from aqueous solution using manganese dioxide-loaded biochar: Behavior and mechanism[J]. Scientific Reports, 2020, 10(1): 6067.

[9] JIA Yang, ZHANG Yingshuang, FU Jiangang, et al. A novel magnetic biochar/MgFe-layered double hydroxides composite removing Pb2+ from aqueous solution: Isotherms, kinetics and thermodynamics[J]. Colloids and Surfaces A: Physicochemical and Engineering Aspects, 2019, 567:278-287.

[10] LIAO Jun, DING Ling, ZHANG Yong, et al. Efficient removal of uranium from wastewater using pig manure biochar: Understanding adsorption and binding mechanisms[J]. Journal of Hazardous Materials, 2022, 423: 127190.

[11] LI Xiangping, WANG Chuanbin, TIAN Jingnan, et al. Comparison of adsorption properties for cadmium

removal from aqueous solution by Enteromorpha prolifera biochar modified with different chemical reagents[J]. Environmental Research, 2020, 186:109502.

[12] KHAN Zulqarnain Haider, GAO Minling, QIU Weiwen, et al. Properties and adsorption mechanism of magnetic biochar modified with molybdenum disulfide for cadmium in aqueous solution[J]. Chemosphere, 2020, 255: 126995.

[13] SHANG Hongru, LI Yinxue, LIU Jingyi, et al. Preparation of nitrogen doped magnesium oxide modified biochar and its sorption efficiency of lead ions in aqueous solution[J]. Bioresource Technology, 2020, 314: 123708.

[14] ZHAO Chenhao, HU Linlin, ZHANG Changai, et al. Preparation of biochar-interpenetrated iron-alginate hydrogel as a pH-independent sorbent for removal of Cr(VI) and Pb(II)[J]. Environmental Pollution, 2021, 287: 117303.

[15] ZHOU Guiyin, LUO Jinming, LIU Chengbin, et al. Efficient heavy metal removal from industrial melting effluent using fixed-bed process based on porous hydrogel adsorbents[J]. Water Research, 2018, 131: 246-254.

[16] LU Ting, MA Ronggang, KE Ke, et al. Synthesis of Gallic acid functionalized magnetic hydrogel beads for enhanced synergistic reduction and adsorption of aqueous chromium[J]. Chemical Engineering Journal, 2021, 408: 127327.

[17] YANG Fan, DU Qing, SUI Long, et al. One-step fabrication of artificial humic acid-functionalized colloid-like magnetic biochar for rapid heavy metal removal[J]. Bioresource Technology, 2021, 328:124825.

[18] CHEN Tao, WEI Yuanfeng, YANG Weijian, et al. Highly efficient As(III) removal in water using millimeter-sized porous granular MgO-biochar with high adsorption capacity[J]. Journal of Hazardous Materials, 2021, 416: 125822.

[19] LIU Yuanhui, TANG Peng, ZHU Yingming, et al. Green aerogel adsorbent for removal of organic compounds in shale gas wastewater: High-performance tuning and adsorption mechanism[J]. Chemical Engineering Journal, 2021, 416: 129100.

[20] CHEN Jian, OUYANG Jinbo, LAI Weixin, et al. Synthesis of ultralight chitosan/activated biochar composite aerogel globules for ketoprofen removal from aqueous solution[J]. Separation and Purification Technology, 2021, 279:119700.

[21] CHEN Jian, OUYANG Jinbo, CAI Xionghui, et al. Removal of ciprofloxacin from water by millimeter-sized sodium alginate/H3PO4 activated corncob-based biochar composite beads[J]. Separation and Purification Technology, 2021, 276:119371.

[22] ZHANG Lixun, GUAN Yuntao. Microbial investigations of new hydrogel-biochar composites as soil amendments for simultaneous nitrogen-use improvement and heavy metal immobilization[J]. Journal of Hazardous Materials, 2022, 424: 127154.

[23] LOW Jingxiang, ZHANG Liuyang, TONG Tong, et al. TiO2/MXene Ti3C2 composite with excellent photocatalytic CO2 reduction activity[J]. Journal of Catalysis, 2018, 361: 255-266.

[24] QU Jianhua, WANG Yuxin, TIAN Xue, et al. KOH-activated porous biochar with high specific surface area for adsorptive removal of chromium(VI) and naphthalene from water: Affecting factors, mechanisms and reusability exploration[J]. Journal of Hazardous Materials, 2021, 401:123292.

[25] NEELI Sai Teja, RAMSURN Hema, NG Chee Yang, et al. Removal of Cr(VI), As(V), Cu(II) and Pb(II) using cellulose biochar supported iron nanoparticles: A kinetic and mechanistic study[J]. Journal of Environmental Chemical Engineering, 2020, 8(5): 103886.

[26] LI Shuaishuai, YANG Fan, LI Jiangshan, et al. Porous biochar-nanoscale zero-valent iron composites: Synthesis, characterization and application for lead ion removal[J]. Science of the Total Environment, 2020, 746: 141037.

[27] HU Zhongting, DING Yin, SHAO Yuchao, et al. Banana peel biochar with nanoflake-assembled structure for cross contamination treatment in water: Interaction behaviors between lead and tetracycline[J]. Chemical Engineering Journal, 2021, 420: 129807.

[28] GAO Ce, WANG Xuelian, AN Qingda, et al. Synergistic preparation of modified alginate aerogel with melamine/chitosan for efficiently selective adsorption of lead ions[J]. Carbohydrate Polymers, 2021, 256: 117564.

[29] LIU Tao, GOU Shaohua, HE Yang, et al. N-methylene phosphonic chitosan aerogels for efficient capture of Cu2+ and Pb2+ from aqueous environment[J]. Carbohydrate Polymers, 2021, 269:118355.

[30] YANG Weixia, CHENG Meijie, HAN Yong, et al. Heavy metal ions' poisoning behavior-inspired etched Uio-66/CTS aerogel for Pb(II) and Cd(II) removal from aqueous and apple juice[J]. Journal of Hazardous

Materials, 2021, 401: 123318.

[31] ZHAO Han, OUYANG Xiaokun, YANG Liye. Adsorption of lead ions from aqueous solutions by porous cellulose nanofiber-sodium alginate hydrogel beads[J]. Journal of Molecular Liquids, 2021, 324: 115122.

[32] LIANG Xuexue, OUYANG Xiaokun, WANG Songyan, et al. Efficient adsorption of Pb(II) from aqueous solutions using aminopropyltriethoxysilane-modified magnetic attapulgite@chitosan (APTS-Fe3O4/APT@CS) composite hydrogel beads[J]. International Journal of Biological Macromolecules, 2019, 137: 741-750.

[33] Dhiss Tesnim, Aida Díez, Hédi Ben Amor, et al. Synthesis and characterization of eco-friendly cathodic electrodes incorporating nano Zero-Valent iron (NZVI) for the electro-fenton treatment of pharmaceutical wastewater[J]. Chemical Engineering Journal, 2024, 502: 158099-158112.

[34] Wang Jianlong, Wang Shizong. Removal of pharmaceuticals and personal care products (PPCPs) from wastewater: A review[J]. Journal of Environmental Management, 2016, 182: 620-640.

[35] Sergio Manzetti, Rossella Ghisi. The environmental release and fate of antibiotics[J]. Marine Pollution Bulletin, 2014, 79 (1-2): 7-15.